Supporting Information

Carbon dopant endows silicon oxide with facilitating redox kinetics of polysulfides

Qiang Zhang,[b] Ranxiao Ao,[ac] Ruijie Gao,[acd,*] Huaming Yang,[abcd,*]

[a] *Engineering Research Center of Nano-Geomaterials of Ministry of Education, China University of Geosciences, Wuhan 430074, China, Email: gaoruijie@cug.edu.cn, hm.yang@cug.edu.cn, Fax: 86-731-88830549, Tel.: 86-731-88710804*

[b] *Hunan Key Laboratory of Mineral Materials and Application, School of Minerals Processing and Bioengineering, Central South University, Changsha 410083, China*

[c] *Faculty of Materials Science and Chemistry, China University of Geosciences, Wuhan 430074, China*

[d] *Key Laboratory of Functional Geomaterials in China Nonmetallic Minerals Industry, China University of Geosciences, Wuhan 430074, China*

[*] Correspondence: gaoruijie@cug.edu.cn (R. Gao, leading contact); hm.yang@cug.edu.cn (H. Yang).

Table of contents

Supplementary Tables

Experimental Section
Materials

Raw graphite mine was obtained from Hunan, China, and raw halloysite was purchased from Sigma-Aldrich (Shanghai) Co., Ltd. Commercial sulfur power, Li_2S, SiC, and N-methyl-2-pyrrolidone (NMP) were purchased from Shanghai Aladdin Bio-Chem Technology Co., Ltd, China. Polyvinylidene difluoride (PVDF, HSV900, ARKEMA), Acetylene black, and ethanol were obtained from Sinopharm Chemical Reagent Co., Ltd, China. All reagents were used without further purification. Ultrapure water (Millipore, 18.23 $M\Omega \cdot cm^{-1}$) was used throughout all of the experiments.

Characterization

The crystal structures of the catalysts were characterized by X-ray diffraction (XRD, Bruker D8 Advance) with Cu $K\alpha$ radiation ($\lambda = 0.15406$ nm) in the 2θ range of 5° to 80°. Raman spectra were performed by Renishaw in Via Raman. Thermogravimetric analyses (TGA) of the catalysts were performed using a METTLER TOLEDO TGA/DSC 3$^+$. The morphologies of the catalysts were investigated using scanning electron microscopy (SEM, TESCAN MIRA4) and transmission electron microscopy (TEM, Titan G260-300) combined with energy dispersive spectroscopy (EDS, Super-X) analysis. The chemical elements and bonding behaviors of the catalysts are investigated using an X-ray photoelectron spectroscopy (XPS, Thermo Scientific K-Alpha). The concentrations of Fe in the leached solutions are measured by the inductively coupled plasma mass spectrometry (ICP-MS, Agilent 7800). Ultraviolet-visible (UV-vis) absorption spectra measurement was tested by Shimadzu UV-3600 plus. Near Edge X-ray Absorption Fine Structure (NEXAFS) was carried out at the Catalysis and Surface Science Endstation at the BL11U beamline in the National Synchrotron Radiation Laboratory (NSRL) in Hefei, China.

Synthesis of C-SiO$_2$

C-SiO$_2$ was prepared by a simple temperature-controlled carbonization process. First, the raw halloysite was washed several times with ultrapure water, and then HCl (6 mol·L^{-1}）was added into the washed halloysite with thermally treated at 90 °C for 6 h. Next, the mixture was washed several times with ultrapure water until neutral and dried at 60 °C for 24 h to obtain the pure activated SiO$_2$. The as-prepared activated SiO$_2$ was carbonized in a tube furnace at 1400 °C for 2 h with powdered graphite mine as the carbon source under an argon atmosphere to obtain C-SiO$_2$-n (n represents catalysts with different proportions of graphite mine and activated SiO$_2$, C-SiO$_2$-4 with the best performance is denoted as C-SiO$_2$ for the readability of the article), and

the synthesis ratio and corresponding catalysts can be seen in Table S1.

Synthesis of C-SiO$_2$/S

The synthesized C-SiO$_2$ and commercial sulfur power were uniformly mixed with a mass ratio of 1:4. The obtained mixture was ground into powder and heated at 155 °C for 12 h under argon atmosphere to synthesize C-SiO$_2$/S. The same method is also used for the fabrication of the sulfur-loaded reference catalysts.

Electrochemical measurements

The Li-S batteries tests were conducted using standard 2016-type coin batteries. To prepare the electrodes for the coin batteries, the C-SiO$_2$/S cathode was homogeneously mixed with conductive acetylene black and PVDF binder in NMP (7:2:1 by weight) to form a slurry that is coated onto a carbon-coated aluminum foil. The same procedures were used to prepare SiO$_2$/S, SiC/S, and C-SiO$_2$-n/S cathodes. The coin batteries were assembled with pure Li meter foils (the diameter of 15.6 mm) as the counter/reference electrodes, Celgard 2400 as the separator, and 1.0 M lithium bis(trifluoromethanesulfonyl) imide (LiTFSI) in 1, 3-dioxolaneand (DOL) and 1, 2-dimethoxyethane (DME) (1:1 by volume) with 0.1 M LiNO$_3$ as the electrolyte. The batteries were all assembled inside a glovebox filled with ultrapure Ar gas, with the water and oxygen concentrations kept below 0.01 p.p.m.. The sulfur cathode batteries were measured with the potential range of 1.5-2.8 V (*vs.* Li$^+$/Li). Galvanostatic charge-discharge (GCD) measurements are conducted at room temperature (25 °C) at various rates on a Land battery tester (Land CT3001A, China) in the voltage range 1.5-2.8 V. Cyclic voltammetry (CV) is performed using an electrochemical workstation (CHI760, Shanghai, China) between 1.5 and 2.8 V at different scan rates. The electrochemical impedance measurements were carried out with electrochemical workstation (CHI760, Shanghai, China) at 5 mV AC oscillation amplitude over the frequency range from 10^5 to 0.01 Hz. The specific capacity is calculated based on the mass of S in the active material.

Visualized adsorption measurements

Typically, the Li$_2$S$_6$ solution (3 mmol·L^{-1}) for visualized adsorption measurements was prepared by mixing sulfur and Li$_2$S at a molar ratio of 5:1 in DOL and DME (1:1 by volume) at 75 °C for 24 h. Then, certain amounts of SiO$_2$, SiC, and C-SiO$_2$ were added to 5 mL of the as-prepared Li$_2$S$_6$ solutions. The UV-vis absorption spectra measurements were performed after soaking the samples into Li$_2$S$_6$ solution for 6 h. All the above operations were carried out in an argon-filled glove box.

Symmetric battery assembly and kinetic evaluation of LiPSs conversion

The electrode was prepared by mixing C-SiO$_2$ and PVDF with a weight ratio of 9:1 in NMP solvent followed by coating the slurry onto a carbon-coated Al foil. The same procedures were used to prepare SiO$_2$ and SiC electrodes. Two identical electrodes were used as the working and the counter electrodes, and Li$_2$S$_6$ was used as electrolyte. The CV measurements of the symmetric batteries were tested with a voltage window between -0.8 to 0.8 V at a scan rate of 50 mV·s^{-1}.

Linear sweep voltammetry measurements

For the reduction of sulfur, the catalysts as the working electrode, the lithium sheet as the reference and counter electrode, 4 mM S$_8$ molecules dissolved in the blank electrolyte as the electrolyte, and the LSV measurements were conducted at a scanning rate of 5 mV·s^{-1} from 2.60 V to 2.35 V. For the oxidation of Li$_2$S, the catalysts as the working electrode, saturated Ag/AgCl as the reference electrode, platinum sheet as the counter electrode, and 0.1 M Li$_2$S/methanol solution as the electrolyte, and the LSV measurements were conducted at a scanning rate of 5 mV·s^{-1} from -0.8 V to -0.15 V.

Li$_2$S nucleation/decomposition measurements

The aforementioned active electrodes and lithium foils were assembled into 2016-type coin batteries as cathodes and counter electrodes, while Celgard 2400 as the separator. 15 μL Li$_2$S$_6$ electrolyte used as catholyte and 15 μL 1.0 M LiTFSI (DOL/DME, 1:1 by volume) as anolyte. Battery assembly was performed in an Ar-filled glovebox by the abovementioned method. For Li$_2$S nucleation, the batteries were galvanostatically discharged at 0.112 mA to 2.06 V and then potentiostatically discharged at 2.05 V for 15 000 s. For Li$_2$S decomposition, the batteries were galvanostatically discharged at 0.112 mA to 1.50 V and then potentiostatically charged at 2.35 V until 15 000 s for the sufficient dissolution of Li$_2$S.

Shuttle current measurements

The electrolyte without LiNO$_3$ additive was employed to prevent the passivation of lithium anode in the shuttle currents measurements. Typically, the assembled batteries were charged and discharged for 3 cycles, and then galvanostatically charged to 2.8 V at the current density of 0.2 C, followed by discharging to 2.38 V and switched to the potentiostatic mode. After around 10 000 s, the potentiostatic current was stabilized at a steady state and can be regarded as shuttle current.

The kinetics measurements of Li$_2$S oxidation

In the homemade beaker battery, the working electrodes are prepared by carbon cloth (CC) coated with synthesized catalysts and Li$_2$S, and the Li foil as the counter and reference

electrode, and 1.0 M LiTFSI in DOL and DME (1:1 by volume) as the electrolyte (Fig. S20). The beaker battery is galvanostatically charged to 2.8 V, while taking some suspension and recording the UV-vis spectra after being centrifuged briefly. The concentrations of Li_2S_6 after reaction are related to the absorption peak at 260 nm and $-lnAbs_{260nm}$ is plotted versus the reaction time, and the apparent rate constants (k_{app}) are obtained from the slope of the data fit as a first-order reaction.

Supplementary Figures
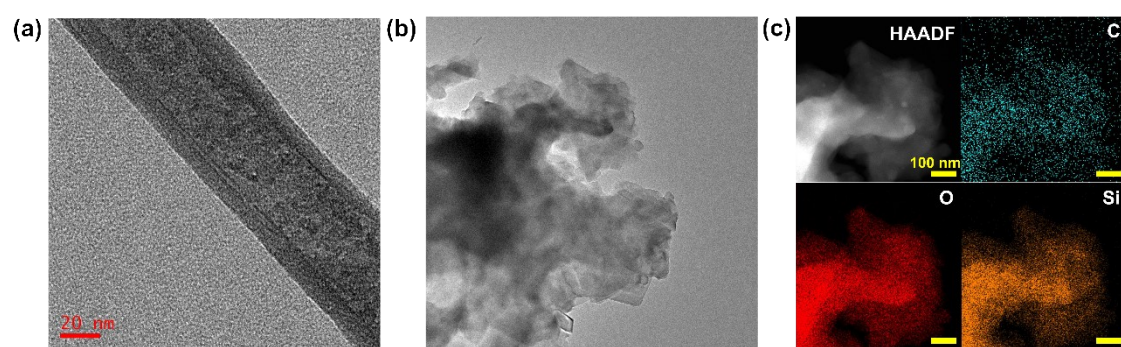
Figure S1. TEM images of (a) raw halloysite and (b) C-SiO$_2$.
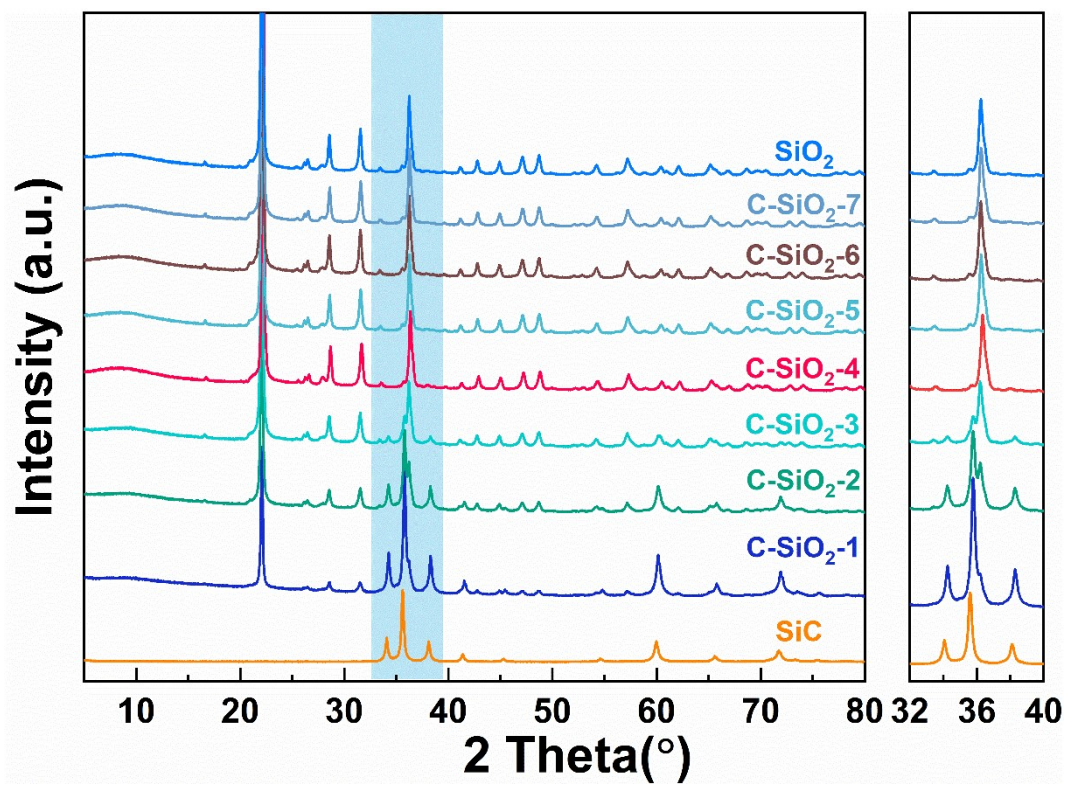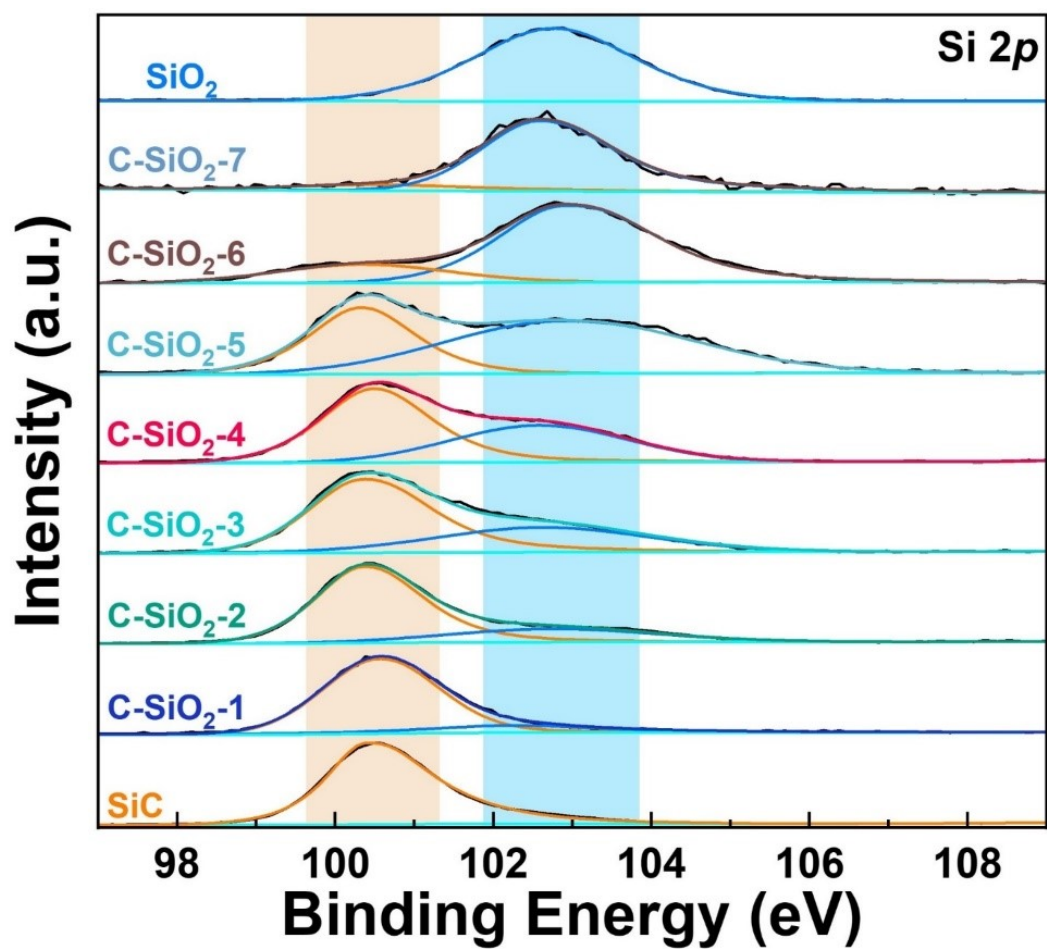
Figure S2. XRD patterns of SiC, SiO_2 and C-SiO_2-n.

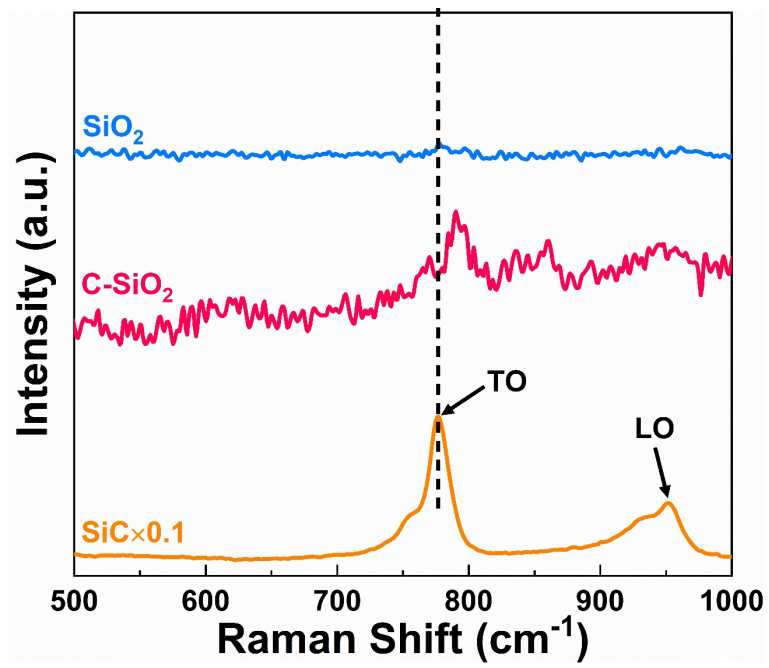**Figure S3.** XPS spectra of SiC, SiO_2 and C-SiO_2-n.

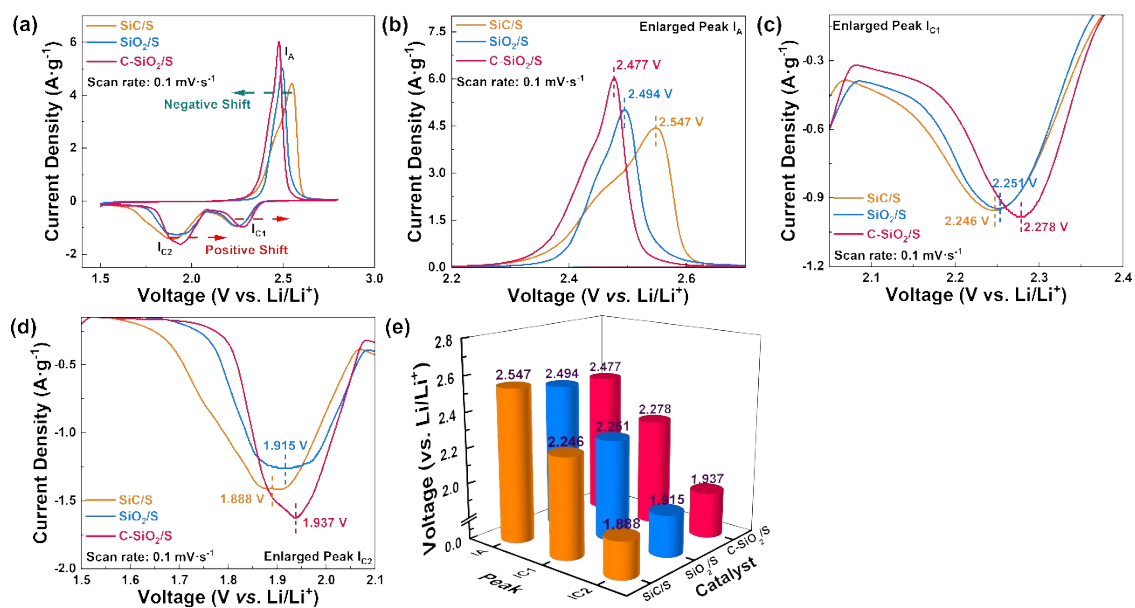**Figure S4.** Raman spectra of synthesized catalysts.

Figure S5. (a) CV curves and the enlarged view in (b) peak I_A and (c) peak I_{C1} and (d) peak I_{C2} of Li-S batteries with different cathodes. (e) Related peak voltages of Li-S batteries acquired by CV plots.
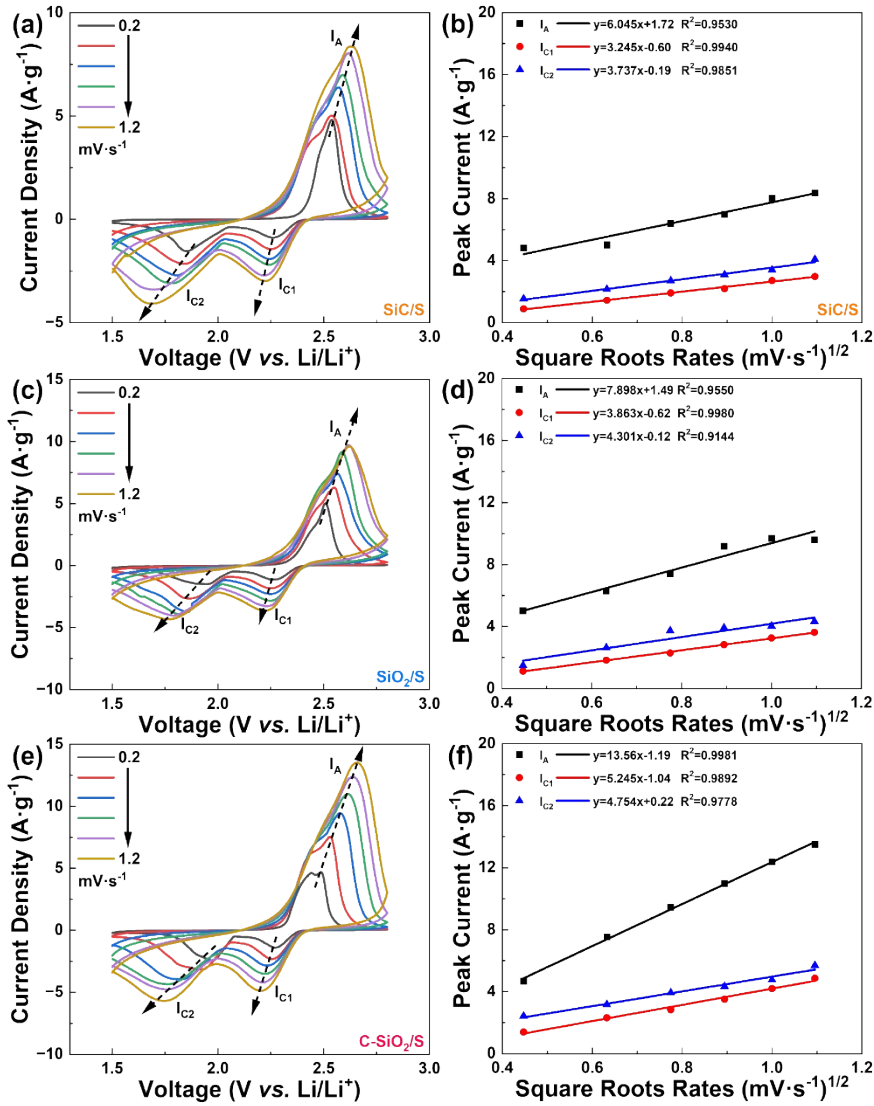
Figure S6. CV curves of Li-S batteries in the voltage ranges of 1.5-2.8 V (*vs*. Li/Li$^+$) at different scan rates from 0.2 to 1.2 mV·s^{-1} for (a) SiC/S, (c) SiO$_2$/S, and (e) C-SiO$_2$/S. The correlation between peak current and the square root of the scan rates for (b) SiC/S, (d) SiO$_2$/S, and (f) C-SiO$_2$/S.

The diffusion coefficient of electrodes can be calculated by the classical Randles-Sevcik equation:[1, 2]

$$I_p = 2.69 \times 10^5 \times n^{3/2} \times A \times D^{1/2} \times C_{Li} \times v^{1/2}$$

where I_p is the peak current (A), n is the charge transfer number ($n = 2$ for Li-S battery), A is the area of cathode (~1.13 cm^2), D is the Li$^+$ diffusion coefficient (cm^2·s^{-1}), C_{Li} is the concentration of Li$^+$ in the material (1 mol·L^{-1}), and v is the scan rate (V·s^{-1}). Because of n, A, and C_{Li} are unchanged, a linear relationship between the peak current (I_{C1}, I_{C2}, I_A) and the square root of scanning rates ($I_p/v^{1/2}$) can represent the lithium-ion diffusion rate.
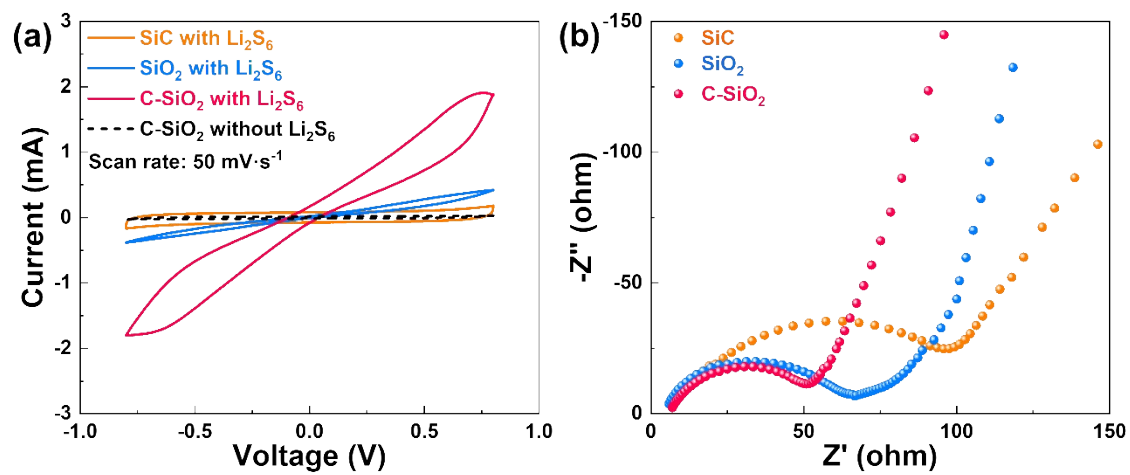
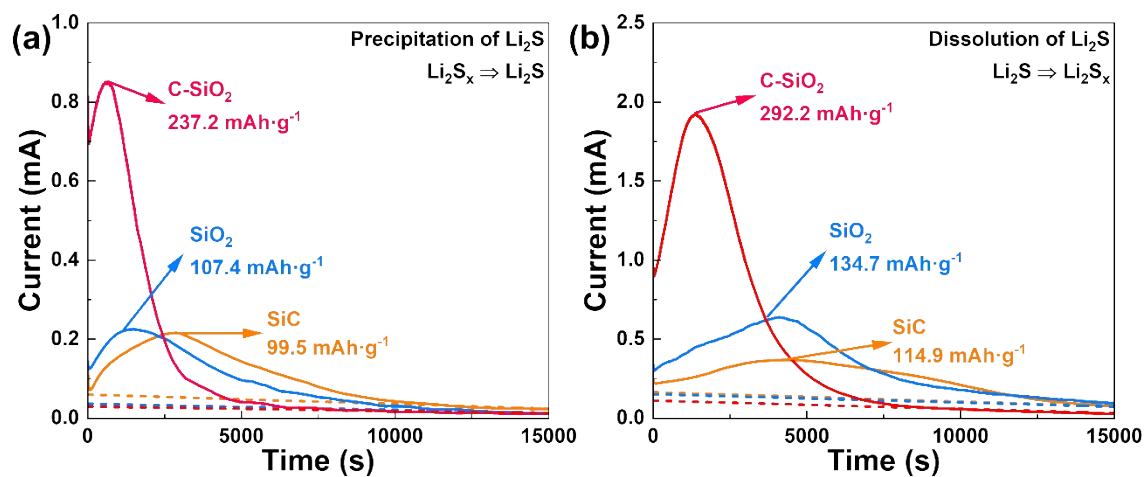**Figure S7.** (a) The CV curves and (b) EIS measurements of symmetric battery.

Figure S8. The current-time plots for potentiostatic (a) discharge and (b) charge profiles of SiC, SiO$_2$ and C-SiO$_2$.
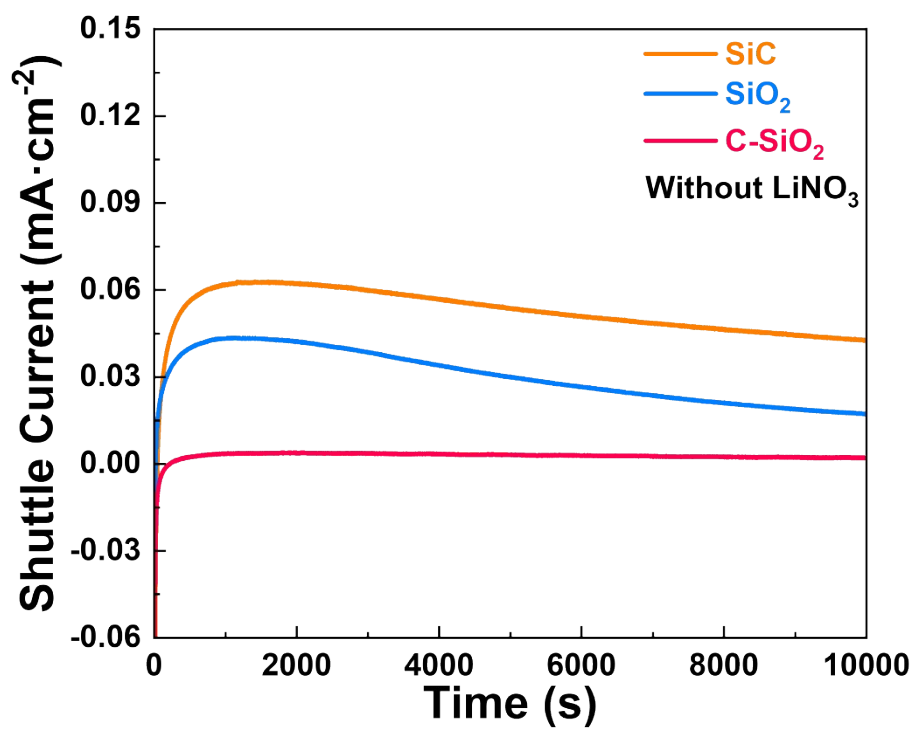
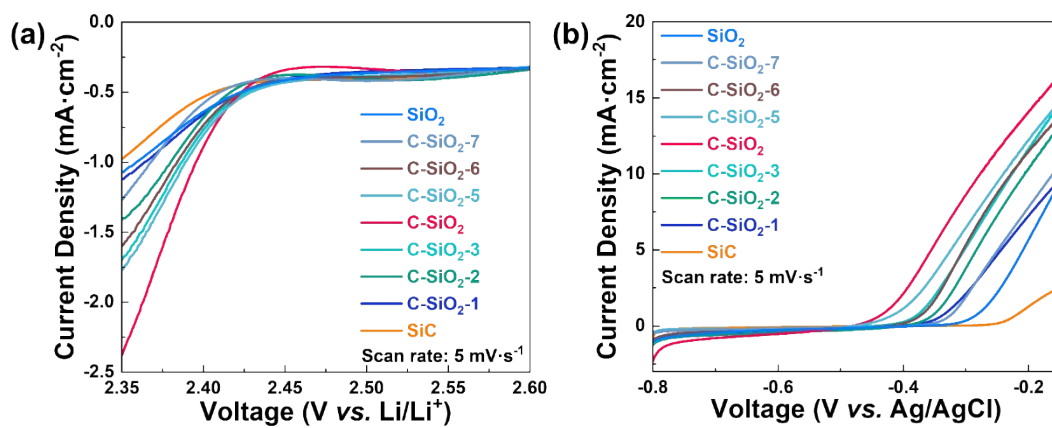**Figure S9.** The shuttle current of SiC, SiO_2 and C-SiO_2.

Figure S10. LSV curves toward (a) sulfur reduction and (b) Li$_2$S oxidation of synthesized catalysts.
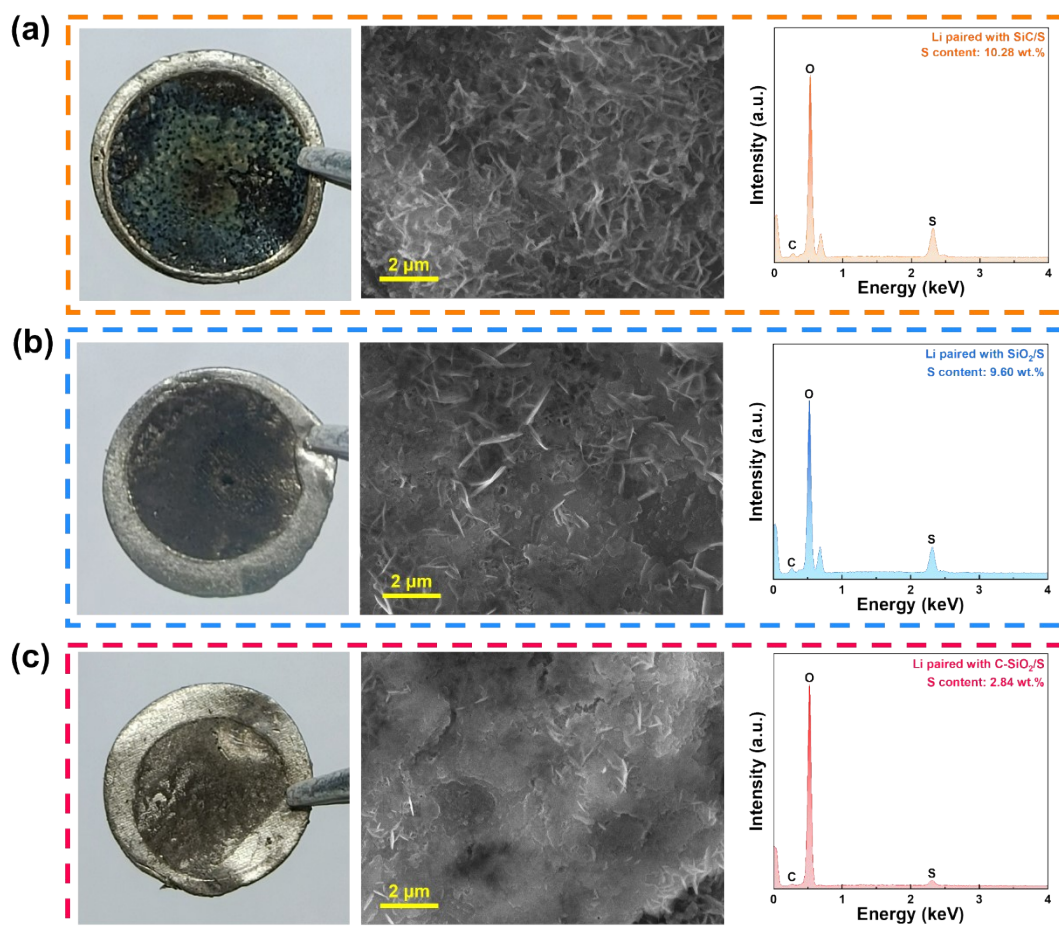
Figure S11. Post-mortem analysis of Li-S batteries after 100 cycles at 0.2 C. Digital photographs, SEM images and corresponding EDS spectra of Li anodes after cycling paired with (a) SiC/S (b) SiO$_2$/S and (c) C-SiO$_2$/S. The batteries were disassembled in an Ar-filled glove box, and Li anodes were washed gently with DME/DOL solvent. After being dried in the glove box at room temperature, Li anodes were transferred into a sealed container for further SEM observations.

The surface of the Li anode is seriously corroded in batteries with SiC/S and SiO$_2$/S cathodes (Supplementary Fig. 11a&b). In contrast, the Li anode with C-SiO$_2$/S cathode maintains a relatively clean appearance, and no obvious LiPSs can be observed (Supplementary Fig. 11c).
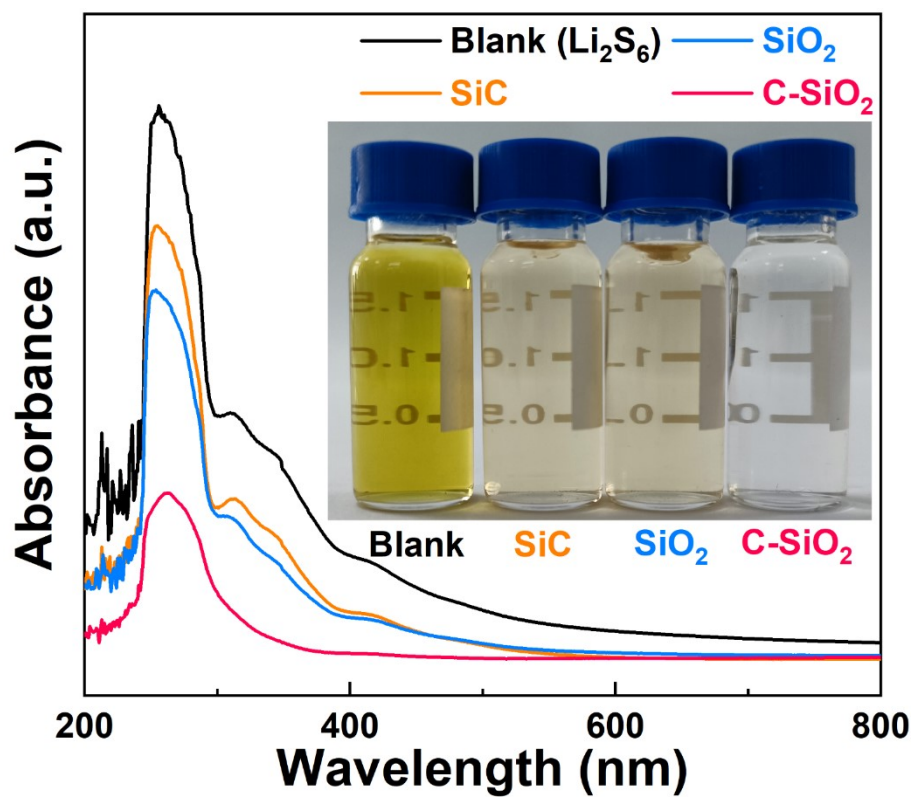
Figure S12. Digital photographs of LiPSs adsorption measurements, and UV-vis spectra with different catalysts after immersion in Li_2S_6 solution.
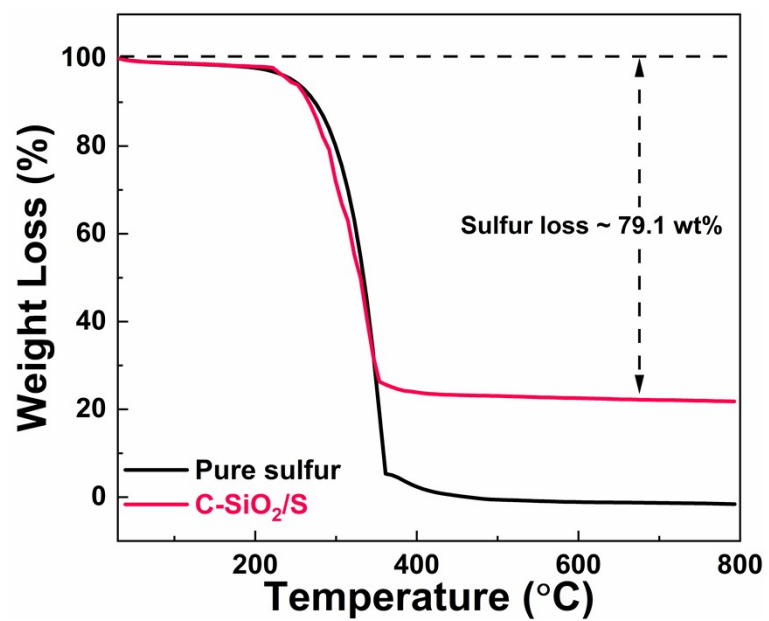
Figure S13. TGA curves of pure sulfur and C-SiO$_2$/S under Ar atmosphere.

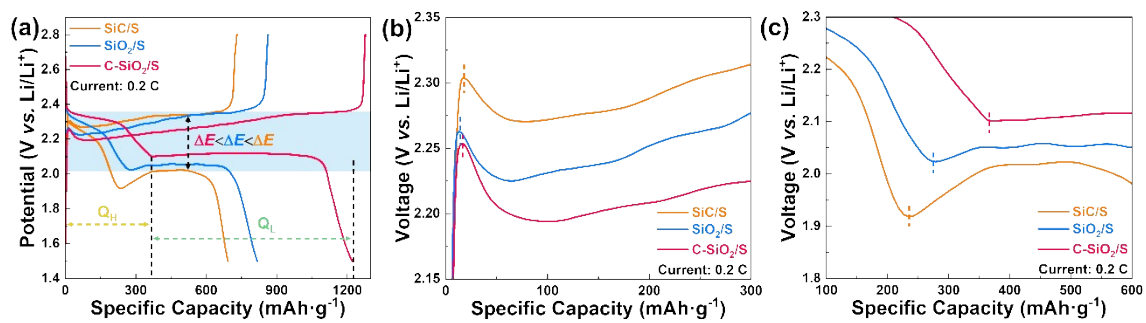**Figure S14.** (a) The galvanostatic charge-discharge curves, and the enlarged view of (b) charge and (c) discharge voltage profiles of the SiC/S, SiO$_2$/S and C-SiO$_2$/S cathodes, respectively.
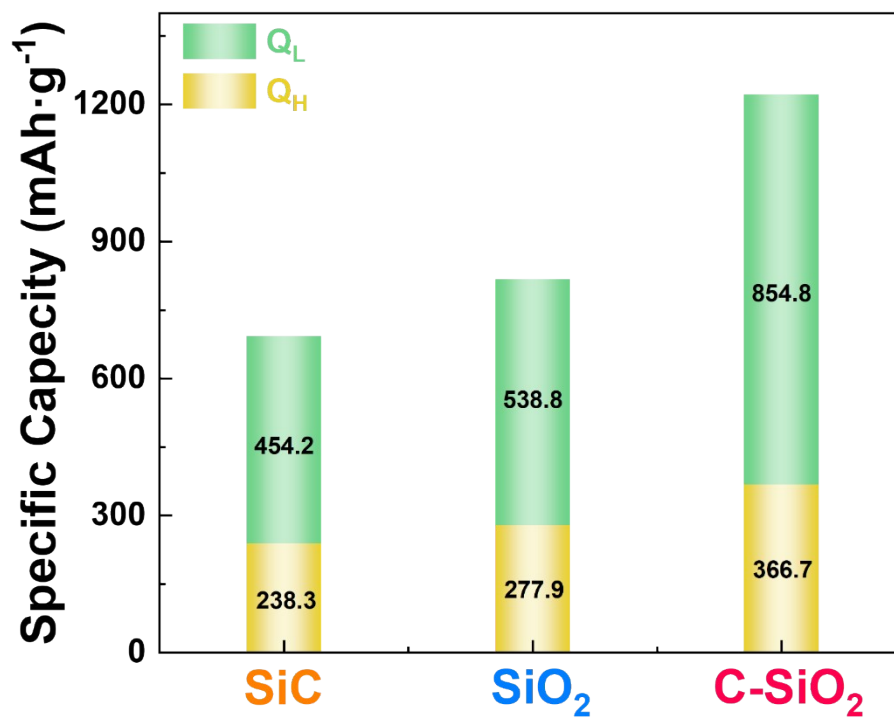
Figure S15. Specific capacity of Li-S batteries with different catalysts at 0.2 C during the first cycle and when combined with ΔQ_H (capacity in 2.1 ~ 2.4 V) and ΔQ_L (capacity in 1.75 ~ 2.1 V).

Figure S16. Cycling performance with C-SiO$_2$/S cathode at 5 C.

The Li-S battery with C-SiO$_2$/S cathode shows a good initial specific capacity of 1009.4 mAh·g^{-1} with a high coulombic efficiency (99.49%) at 5.0 C, and the specific capacity still maintains 835 mAh·g^{-1} even after 100 cycles.

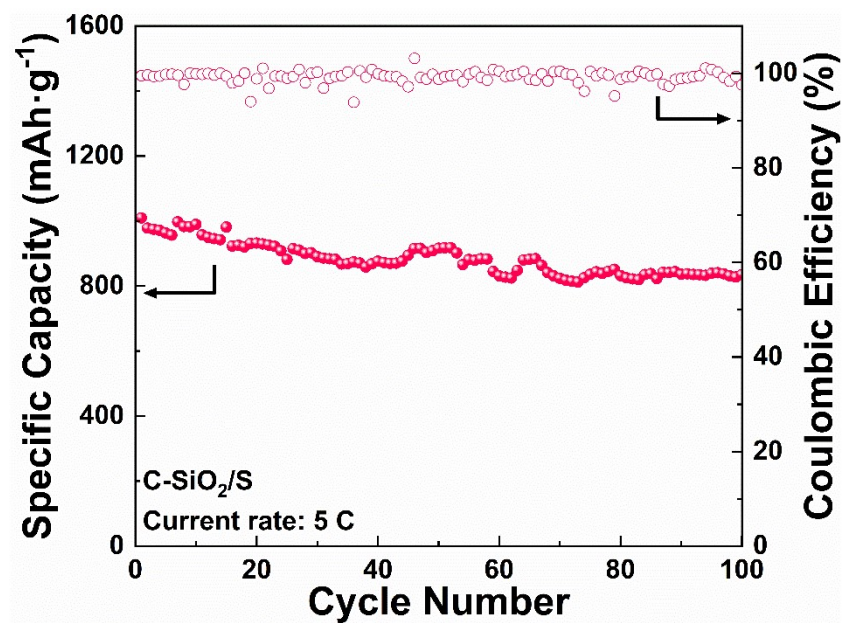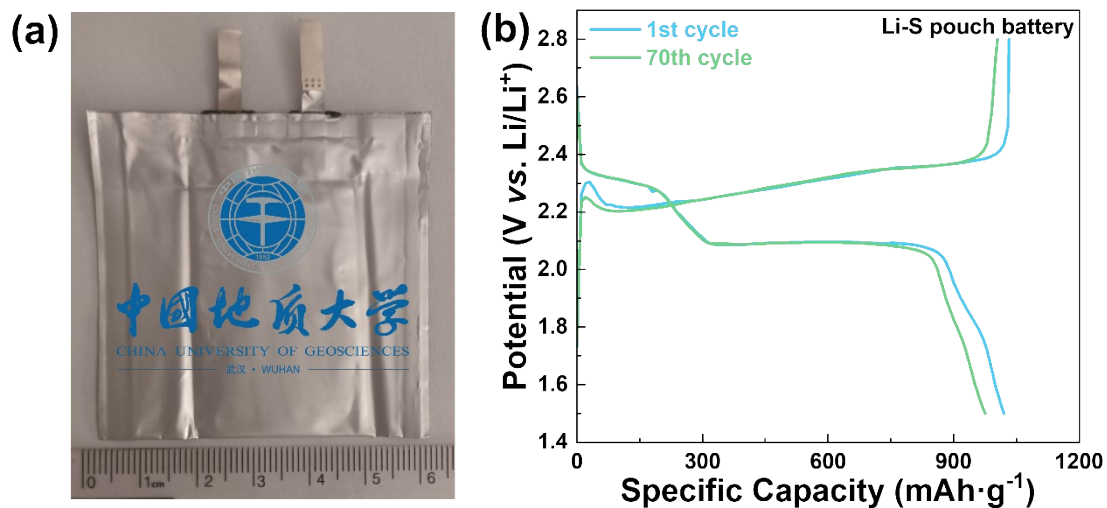**Figure S17.** (a) Digital photo of the as-prepared Li-S pouch battery and the Li anode (30 mm× 45 mm) is slightly larger than the cathode (28 mm × 40 mm, China University of Geosciences badge: permission for use obtained from China University of Geosciences). (b) The galvanostatic charge-discharge curves of the 1st cycle and the 70th cycle of Li-S pouch battery fabricated with the C-SiO$_2$/S cathode at 0.1 C.
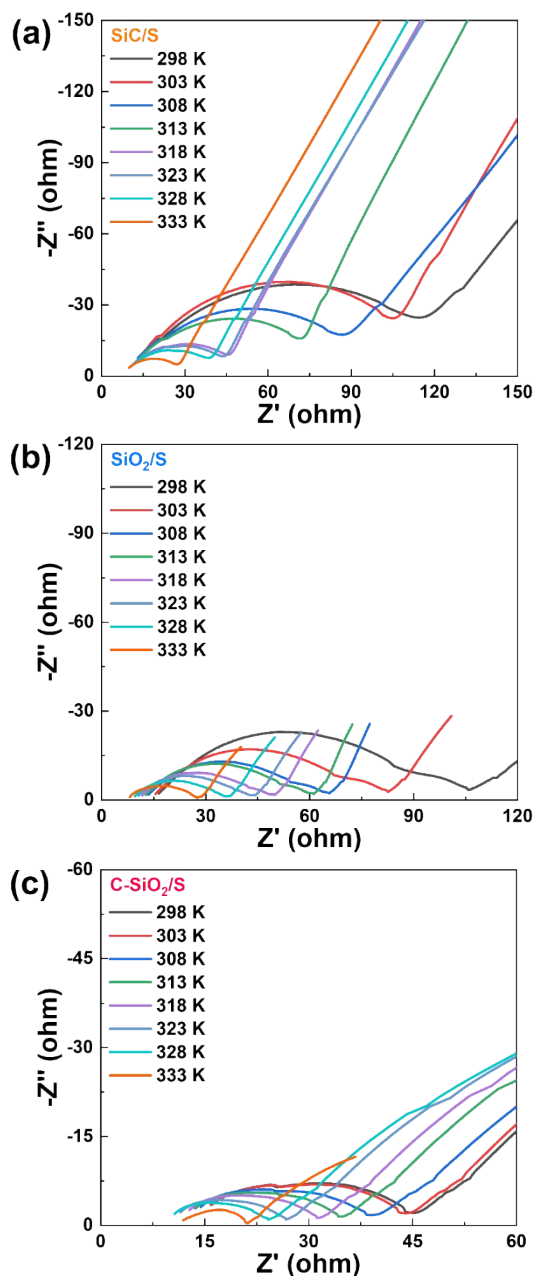
Figure S18. Charge transfer resistance of S reduction reaction at various temperatures among (a) SiC/S, (b) SiO$_2$/S and (c) C-SiO$_2$/S cathodes at the onset potential.

The activation energy barrier (E_a) can be extracted based on the Arrhenius equation, which is interrelated with the transportation kinetics of ion/electron from the active centers that are engaging in SRR.[3, 4]
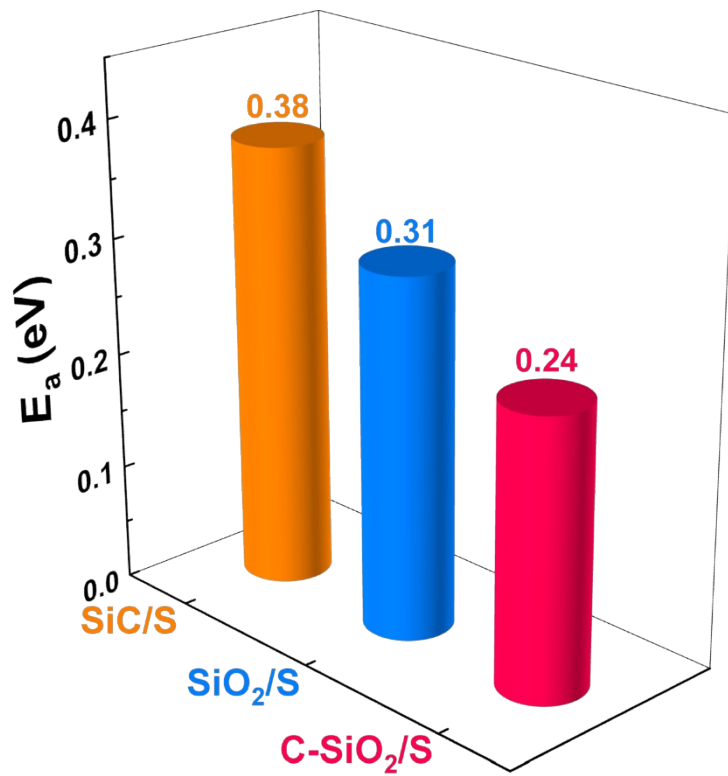
Figure S19. The E_a for different cathodes at OCV.
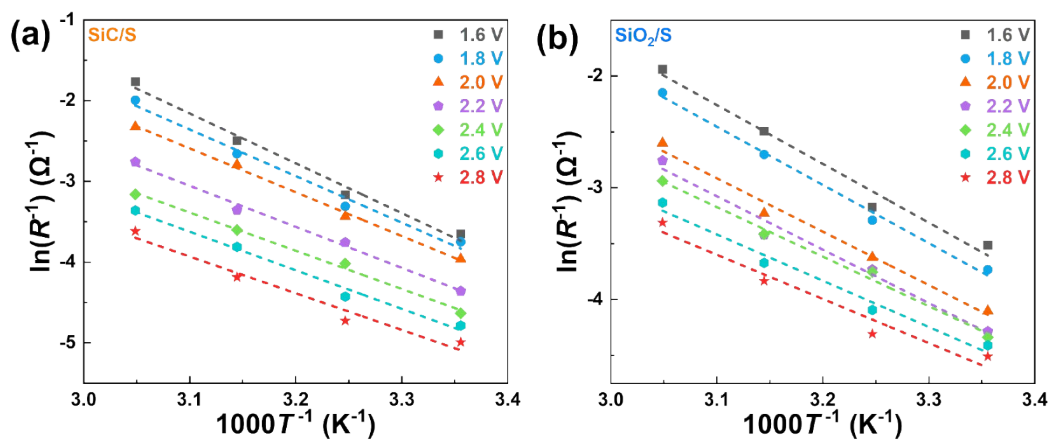
Figure S20. Arrhenius plot showing the linear relationship between logarithmic values of the reciprocal of charge transfer resistance and the reciprocal of absolute temperatures for (a) SiC/S and (b) SiO$_2$/S cathodes.
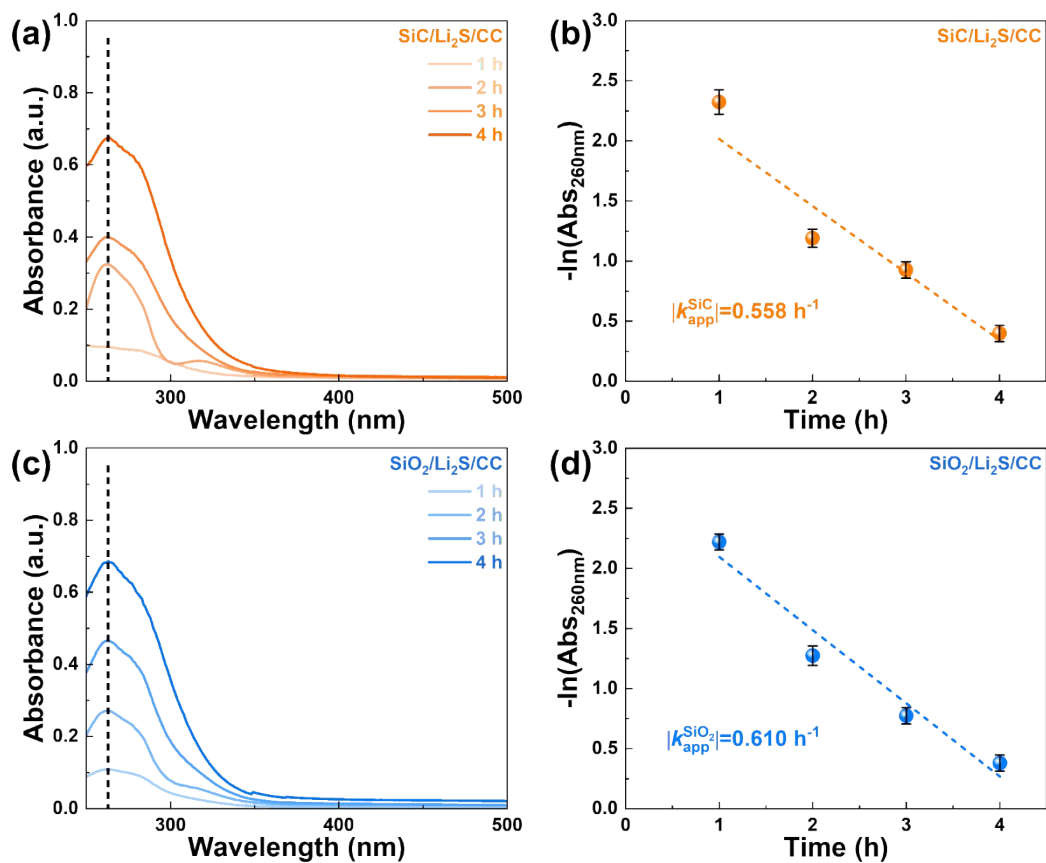
Figure S21. Measurement of k_{app} using UV-vis spectrometry in reactions of different catalysts oxidizing Li$_2$S after various times in electrolyte. Error bars represent standard deviations of at least three measurements.
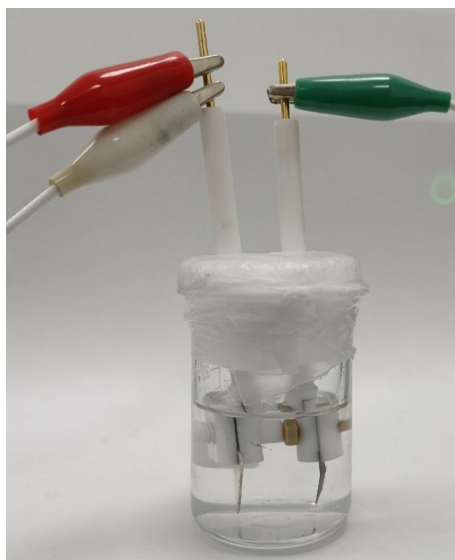
Figure S22. Optical image of the *in situ* beaker battery observation experiments.

Supplementary Tables
Table S1. Mass ratio and the corresponding catalyst

SiO$_2$:C (wt%)	Catalysts
0.2	C-SiO$_2$-1
0.5	C-SiO$_2$-2
1.0	C-SiO$_2$-3
1.5	C-SiO$_2$-4
2.0	C-SiO$_2$-5
3.0	C-SiO$_2$-6
5.0	C-SiO$_2$-7

Table S2. Electrochemical performance comparison for Li-S coin batteries.

Materials Type	Rate (C)	Capacity (mAh·g^{-1})	Ref.
S@Co$_9$S$_8$	1	756.6 (600th)	5
NCO-HS	0.2	1143.8 (100th)	6
N-CoSe$_2$/S	0.2	924 (250th)	7
S/CoZn-Se@N-MX	0.2	1016 (100th)	8
S/Fe-N$_5$-C	0.2	920.4 (100th)	9
Fe$_3$C-S@C@Fe$_3$C	1	620 (370th)	10
a-Ta$_2$O$_{5-x}$/MCN/S	1	680 (1000th)	11
EFG-S	0.5	650 (350th)	12
Li$_2$S@graphene	0.1	762 (200th)	13
S@Co-N/G	1	681 (500th)	14
S@WLC-CNTs	0.2	~613 (200th)	15
Li$_2$S@Co-C@CHF	0.2	~729 (200th)	16
NSHG/S$_8$/NiCF	0.5	~747 (400th)	17
C-SiO$_2$	**0.2**	**1105.8 (200th)**	**This work**
	2	**654.4 (750th)**	

Table S3. Electrochemical performance comparison with high areal sulfur loading for Li-S coin batteries.

Materials Type	S loading (mg·cm^{-2})	Rate	Areal capacity (mAh·cm^{-1})	Ref.
S@CoNi-MOF	4.6	0.1 C	4.14 (80th)	4
S/Fe-N$_5$-C	4.3	0.1 C	4.4 (50th)	9
NSHG/S$_8$/NiCF	3.2	2 mA • cm^{-2} (0.37 C)	2.01 (100th)	17
{Co$_4$W$_{18}$}/rGO/S	5.6	0.1 C	4.55 (50th)	18
G@ppy-por	5.0	0.2 C	4.0 (50th)	19
C-SiO$_2$	**5.23**	**0.2 C**	**5.19 (100th)**	**This work**

Table S4 Electrochemical performance comparison for Li-S pouch batteries.

Materials	Areal S loading (mg·cm^{-2})	Areal capacity (mAh·cm^{-2})	Ref.
G@ppy-por	7.0	~7.64 (12th)	19
Mo_6S_8	6.9	7.54 (10th)	20
CNT aerogel@Li_2S_8	10	10.4 (20th)	21
alucone-coated C-S	2.95	2.86 (1th)	22
ICFs/nS/rGO	7.56	8.75 (51th)	23
DPDSe	4.9	~5.7 (30th)	24
VS_4@RGO	5	3.65 (50th)	25
C-SiO$_2$	**5.63**	**5.49** (70th)	**This work**

Supplementary references

1   Q. Zhang, R. Gao, Z. Li, B. Zhou, A. Tang, J. Wang, J. J. Zou and H. Yang, *Small*, 2022, **18**, 2105661.
2. G. Zhou, H. Tian, Y. Jin, X. Tao, B. Liu, R. Zhang, Z. W. Seh, D. Zhuo, Y. Liu, J. Sun, J. Zhao, C. Zu, D. S. Wu, Q. Zhang and Y. Cui, *Proc. Natl. Acad. Sci. U.S.A.*, 2017, **114**, 840-845.
3. L. L. Peng, Z. Y. Wei, C. Z. Wan, J. Li, Z. Chen, D. Zhu, D. Baumann, H. T. Liu, C. S. Allen, X. Xu, A. I. Kirkland, I. Shakir, Z. Almutairi, S. Tolbert, B. Dunn, Y. Huang, P. Sautet and X. F. Duan, *Nat. Catal.*, 2020, **3**, 762-770.
4. R. J. Meng, Q. J. Du, N. Zhong, X. Zhou, S. H. Liu, S. F. Yin and X. Liang, *Adv. Energy Mater.*, 2021, **11**.
5. C. L. Dai, J. M. Lim, M. Q. Wang, L. Y. Hu, Y. M. Chen, Z. Y. Chen, H. Chen, S. J. Bao, B. L. Shen, Y. Li, G. Henkelman and M. W. Xu, *Adv. Funct. Mater.*, 2018, **28**, 1704443.
6. D. Luo, G. Li, Y. P. Deng, Z. Zhang, J. Li, R. Liang, M. Li, Y. Jiang, W. Zhang, Y. Liu, W. Lei, A. Yu and Z. Chen, *Adv. Energy Mater.*, 2019, **9**.
7. M. Wang, L. Fan, X. Sun, B. Guan, B. Jiang, X. Wu, D. Tian, K. Sun, Y. Qiu, X. Yin, Y. Zhang and N. Zhang, *ACS Energy Lett.*, 2020, **5**, 3041-3050.
8. Z. Ye, Y. Jiang, L. Li, F. Wu and R. Chen, *Adv. Mater.*, 2021, **33**, 2101204.
9. Y. Zhang, J. Liu, J. Wang, Y. Zhao, D. Luo, A. Yu, X. Wang and Z. Chen, *Angew. Chem. Int. Ed.*, 2021, **60**, 26622-26629.
10. W. Weng, J. Xiao, Y. Shen, X. Liang, T. Lv and W. Xiao, *Angew. Chem. Int. Ed.*, 2021, **60**, 24905-24909.
11. Z. Zhang, D. Luo, G. R. Li, R. Gao, M. Li, S. Li, L. Zhao, H. Z. Dou, G. B. Wen, S. Sy, Y. F. Hu, J. D. Li, A. P. Yu and Z. W. Chen, *Matter*, 2020, **3**, 920-934.
12. Z. Wang, Y. Dong, H. Li, Z. Zhao, H. B. Wu, C. Hao, S. Liu, J. Qiu and X. W. Lou, *Nat. Commun.*, 2014, **5**, 5002.
13. G. Tan, R. Xu, Z. Xing, Y. Yuan, J. Lu, J. Wen, C. Liu, L. Ma, C. Zhan, Q. Liu, T. Wu, Z. Jian, R. Shahbazian-Yassar, Y. Ren, D. J. Miller, L. A. Curtiss, X. Ji and K. Amine, *Nat. Energy*, 2017, **2**.
14. Z. Du, X. Chen, W. Hu, C. Chuang, S. Xie, A. Hu, W. Yan, X. Kong, X. Wu, H. Ji and L. J. Wan, *J. Am. Chem. Soc.*, 2019, **141**, 3977-3985.
15. N. Wang, X. Zhang, Z. Ju, X. Yu, Y. Wang, Y. Du, Z. Bai, S. Dou and G. Yu, *Nat. Commun.*, 2021, **12**, 4519.
16. Y. Liu, X. Meng, Z. Wang and J. Qiu, *Sci. Adv.*, 2022, **8**, 1.
17. J. Chang, J. Shang, Y. Sun, L. K. Ono, D. Wang, Z. Ma, Q. Huang, D. Chen, G. Liu, Y. Cui, Y. Qi and Z. Zheng, *Nat. Commun.*, 2018, **9**, 4480.
18. J. Lei, X. X. Fan, T. Liu, P. Xu, Q. Hou, K. Li, R. M. Yuan, M. S. Zheng, Q. F. Dong and J. J. Chen, *Nat. Commun.*, 2022, **13**, 202.
19. C. X. Zhao, X. Y. Li, M. Zhao, Z. X. Chen, Y. W. Song, W. J. Chen, J. N. Liu, B. Wang, X. Q. Zhang, C. M. Chen, B. Q. Li, J. Q. Huang and Q. Zhang, *J. Am. Chem. Soc.*, 2021, **143**, 19865-19872.
20. W. Xue, Z. Shi, L. Suo, C. Wang, Z. Wang, H. Wang, K. P. So, A. Maurano, D. Yu, Y. Chen, L. Qie, Z. Zhu, G. Xu, J. Kong and J. Li, *Nat. Energy*, 2019, **4**, 374-382.
21. Z. Fang, Y. Luo, H. Wu, L. Yan, F. Zhao, Q. Li, S. Fan and J. Wang, *Carbon*, 2020, **166**, 183-192.
22. X. Li, M. Banis, A. Lushington, X. Yang, Q. Sun, Y. Zhao, C. Liu, Q. Li, B. Wang, W. Xiao, C. Wang, M. Li, J. Liang, R. Li, Y. Hu, L. Goncharova, H. Zhang, T. K. Sham and X. Sun, *Nat. Commun.*, 2018, **9**, 4509.
23. F. Wu, Y. S. Ye, J. Q. Huang, T. Zhao, J. Qian, Y. Y. Zhao, L. Li, L. Wei, R. Luo, Y. X. Huang, Y. Xing and R. J. Chen, *ACS Nano*, 2017, **11**, 4694-4702.
24. M. Zhao, X. Chen, X. Y. Li, B. Q. Li and J. Q. Huang, *Adv. Mater.*, 2021, **33**, 2007298.
25. L. Luo, J. Li, H. Yaghoobnejad Asl and A. Manthiram, *ACS Energy Lett.*, 2020, **5**, 1177-1185.